Chapter 25

Ionic-Liquid-Assisted Synthesis of Hierarchical Ceramic Nanomaterials as Nanofillers for Electromagnetic-Absorbing Coatings

Elaheh Kowsari

Additional information is available at the end of the chapter

http://dx.doi.org/10.5772/51653

1. Introduction

The use of electronic devices is experiencing an exponential growth in all the fields of human life, and most of them (personal computers, communication, medical and analytic devices, a lot of domestic appliances) work in the microwave frequency range. This growth gives rise to an increase of Electro Magnetic Interference (EMI) so that it is mandatory to develop systems to protect electronic devices from external interferences.

Electromagnetic (EM) wave absorption materials have attracted much attention owing to the expanded EM interference problems. The EM absorbers are now requested to have not only strong absorption characteristics and wide absorption frequency, but also light weight and antioxidation. The electric permittivity (ε) and magnetic permeability (μ) are parameters related to the dielectric and magnetic properties of a material, and directly associated to their absorbing characteristics [1-5].

The relative permittivity and permeability are represented by Equations 1 and 2, respectively; the values of these parameters are calculated from the experimental values of the transmission and refection coeffcients of the material.

$$\varepsilon_r = \varepsilon' + i\varepsilon'' \tag{1}$$

$$\mu_r = \mu' + i\mu'' \tag{2}$$

In these equations, the primed and double-primed symbols denote real and imaginary components. When the material is lossy, the permittivity and permeability of are complex and some of the incident electromagnetic energy is dissipated [6-7].

In the case of a magnetic material, losses are produced by changes in the alignment and rotation of the magnetization spin [1,8, 9].

The traditional absorbers such as ferrite have strong absorption characteristics, but the thickness required is too large. Therefore, many nanostructures have recently been studied for attenuation of EM wave. These materials are involved with carbon nanotubes, iron and zinc oxide, etc [10-14]. EM wave absorption capability depends on the nature, shape, and size of an absorber.

The dramatic effect that shape anisotropy has on the electronic, optical, and catalytic properties of noble ceramic nanostructures makes the development of morphology-controlled synthesis strategies a main step toward the design of future nanodevices [15-19].

In this regard, the last years have been very prolific in the design of new procedures dealing with the synthesis of noble metal anisotropic structures (Au, Ag, Pt, Pd) such as nanowires, [20-22] nanoplates, [23-26] nanocubes, [27,28] and nanorods [29] with well-controlled size. Recently, some examples concerning the synthesis of branched nanostructures (monopod,bipod, tripod, tetrapod,multipod),[30-35] star polyhedral crystals [36], nanoflowers [37], and ringlike nanostructures[38] have also been reported.

Hierarchical nano-/micro-structures with specific morphology have fascinated scientists all over the world because of their sophisticated architectures which are expected to provide some unique and exciting properties. To date, many recent efforts have been devoted to the synthesis of inorganic materials with hierarchical shapes, including metal [39,40], metal oxide [41], sulfide [42], hydrate [43], and other minerals [44,45].

Recently, ionic liquids have aroused increasing interest because of their unique properties and the potential applications. Ionic liquid can act as a new reaction medium for reactants and morphology templates for the products at the same time, which enables the synthesis of hierarchical nano-/micro-structures with novel or improved properties [46]. Novel nanostructures can be produced by selecting suitable ionic liquids reaction systems. Various nano- or microstructured materials, such as Bi_2S_3 nanostructures [47, 48],Bi_2Se_3 nanosheets [49] and hollow TiO_2 microspheres [50] have been synthesized in ionic liquids.

In this chapter, an attempt has been made to develop hierarchical ceramic nanomaterials with a wide range of morphologies and sizes with improved reflection losses (RL). The duration of experimental processes parameters like amount of IL, pH and temperature have been extensively optimized to obtain morphologies and sizes.

1.1. Development of Innovative Synthesis Methods of Ceramic Nano-materials Using Ionic Liquid

Synthesis of nanomaterials is an increasing active area [51,52]. This interest arises from not only their unusual chemical and physical properties but also their potential application in

http://dx.doi.org/10.5772/51653

many fields, which have stimulated the search for new synthetic methods for these materials. Size, morphology and dimensionality can strongly affect the properties of nanostructured materials. Recently, nanostructured metallic and semiconducting materials with various structures and morphologies have received muchattention due to their novel applications, intriguing properties, and quantum size effects [53]. Especially, a three-dimensional (3D) integrated platform of nanostructured materials is highly desirable for applications in advanced nanoelectronic, optoelectronic, solar cells, sensor, etc., [54–56].

Novel nanostructures can be produced by selecting suitable ILs reaction systems. Various nano- or microstructured materials, have been synthesized in ILs

Cupric oxide (CuO) with leaf-like, chrysanthemum-like and rod shapes have been synthesized by microwave-assisted approach using an ionic liquid 1-n-butyl-3-methyl imidazolium tetrafluoroborate ([BMIM]BF4) by Xu and coworkers [57]. By controlling the concentration of [BMIM]BF_4 and reaction time, shape transformation of CuO nanostructures could be achieved in a short period of time. The morphologies of the samples were shown in Figure. 1. Leaf-like CuO nanosheets with uniform shape and size were obtained on a large scale (Figure. 1(a)).

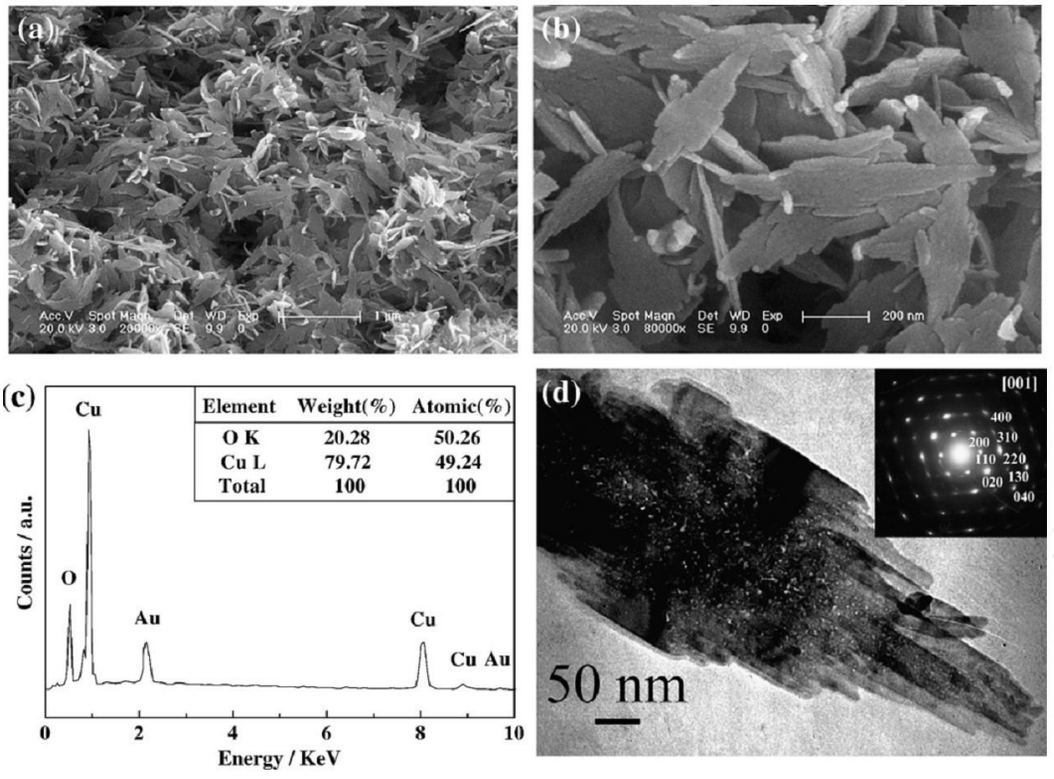

Figure 1. FESEM images of sample A (a–b), EDS results of sample A (c), and TEM image of sample A (d). The inset showed the SAED pattern taken from d.(Reproduced from X Xu, M Zhang, J Feng, M Zhang. Shape-controlled synthesis of single-crystalline cupric oxide by microwave heating using an ionic liquid. Mat Lett. 2008; 62:2787–2790, Copyright (2008), with permeation from Elsevier).

MoS_2 microspheres were successfully synthesized via a facile hydrothermal route assisted by an ionic liquid [BMIM][BF4] by Ma and coworkers [58]. SEM images showed that the MoS_2 mi-

crospheres had uniform sizes with mean diameter about 2.1 μm. The MoS_2 microspheres had rough surfaces and were constructed with sheetlike structures. Ionic liquid played a crucial role as a templating reagent in the formation of MoS_2 microspheres. A possible formation mechanism of MoS_2 microspheres was preliminarily presented. The size and morphology of the samples were examined by SEM. Figure. 2A shows that the as-synthesized MoS_2 products display a uniform spherical morphology with mean diameter of 2.1 μm.

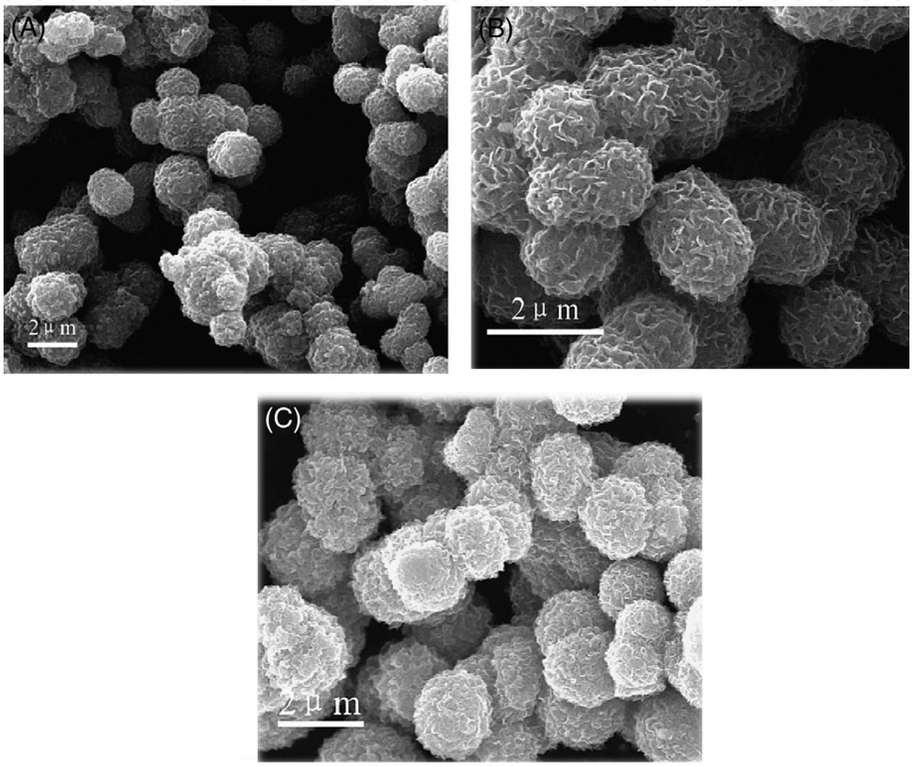

Figure 2. SEM images of MoS2 microspheres prepared by IL-assisted hydrothermal process. (A) and (B) as-synthesized samples and (C) after annealing at 800 °C for 2 h. [Reproduced from Ma L, Chen WX, Li H, Zheng YF, Xu ZD. Ionic Liquid-Assisted Hydrothermal Synthesis of MoS2 Microspheres. Mat Lett. 2008; 62: 797–799, Copyright (2008), with permeation from Elsevier)].

Wurtzite CdSe nanoparticles-assembled microspheres with macropores have been successfully synthesized through a modified hydrothermal method with $Cd(NO_3)_2$ and Na_2SeO_3 as precursors and hydrazine hydrate as a reductant in the presence of 1-n-butyl-3-methylimidazolium bromide ([Bmim]Br) by Liu and coworkers [59]. The results indicated that the CdSe microspheres have an average size of about 3 μm and were assembled by CdSe nanoparticles with size ranging from 20 to 40 nm. It was found that the pH and [Bmim]Br have influence on the morphologies of the products. Figure. 3 shows Wurtzite CdSe nanoparticles-assembled microspheres.

ZnO/SnO_2 nanostructured have been successfully synthesized by a hydrothermal method in the presence of the chiral ionic liquid (CIL) ditetrabutylammonium tartrate, [TBA]2[L-Tar] by Kowsari and coworkers [60].The results revealed that using different ratios of

http://dx.doi.org/10.5772/51653

Zn^{2+}/Sn^{4+} affects the phase and morphology of the ZnO/SnO_2 nanocomposite materials. Figure. 4 shows ZnO/SnO_2 nanostructures.

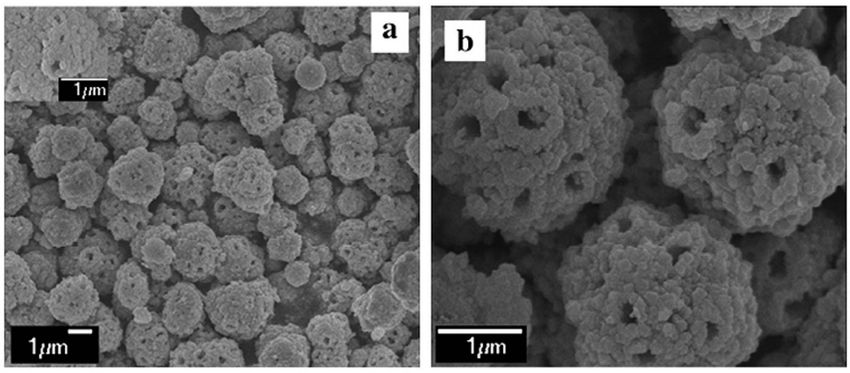

Figure 3. (a) Low magnification SEM image of the CdSe microspheres, the inset shows the structure on the surface of the microspheres; (b) Magnified SEM image of three individual CdSe microspheres. [Reproduced from Liu X, Peng P, Ma J, Zheng W. Preparation of novel CdSe microstructure by modified hydrothermal method. Mat Lett. 2009; 63: 673–675. ,Copyright (2009), with permeation from Elsevier)].

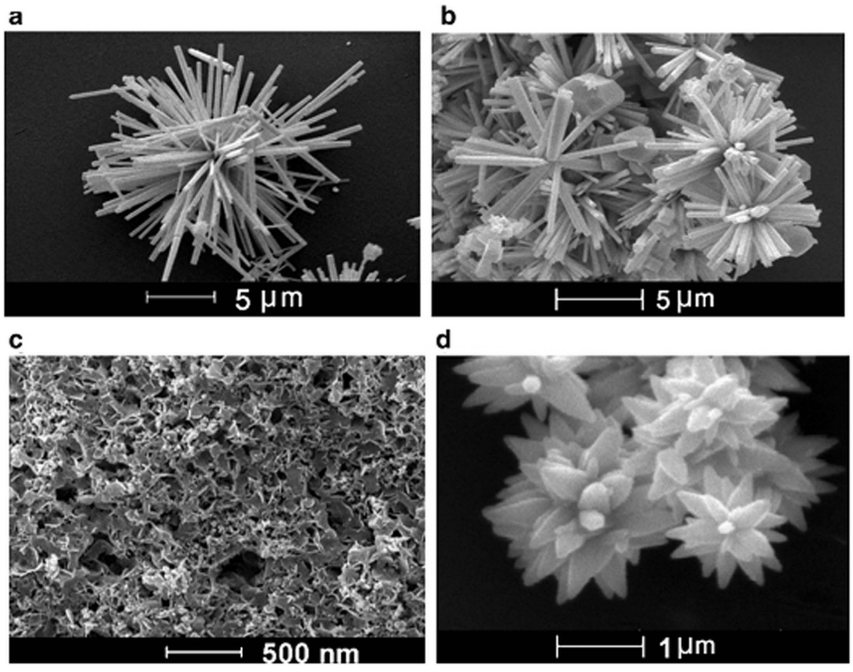

Figure 4. SEM images of products obtained at different Zn^{2+}/Sn^{4+} molar ratios: (a) 2:1, (b) 1:1, (c) 4:1, (d) 1:2, (e) 0:1, and (f) 1:0; the reaction time was kept constant at 24 h and the reaction temperature was 170 °C, CIL=0.05 g. [Reproduced from Kowsari E, Ghezelbash MR. Ionic liquid-assisted, Facile Synthesis of ZnO/SnO_2 Nanocomposites, and Investigation of Their Photocatalytic Activity. Mat Lett. 2012; 68: 17–20,Copyright (2009), with permeation from Elsevier)].

A hydrothermal method has been employed to prepare cactus-like zincoxysulfide ZnO_xS_{1-x} nanostructures with the assistance of a dicationic task-specific ionic liquid (TSIL), [mim]$\{(CH)_2\}_3$[imm]$(SCN)_2$ by kowsari and coworkers[61]. To the best of our knowledge, this is the

first time that this TSIL with the SCN anion has been used in place of conventional reagents as a source of S to prepare a ZnO_xS_{1-x} nanostructure. The effect of the TSIL concentration on the morphology of the products shows in Figure. 5.

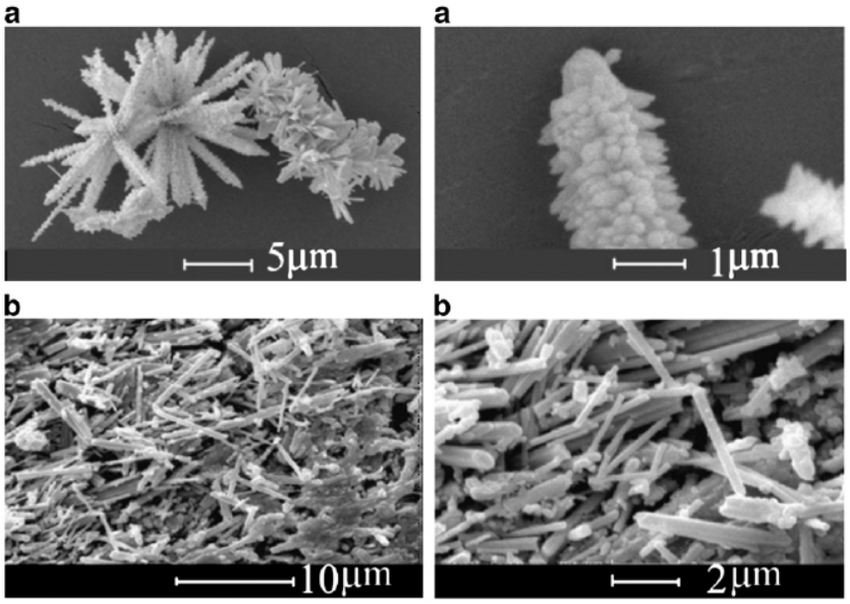

Figure 5. SEM images of products obtained with different amounts of FIL: (a) 0.22 g (S-1), (b) 0.1 g (S-2); the reaction time was constant at 24 h and Zn2+/OH−=1:20; the reaction temperature was 170 °C. [Reproduced from Kowsari E, Ghezelbash MR. Synthesis of Cactus-Like Zincoxysulfide (ZnO_xS_{1-x}) Nanostructures Assisted by a Task-Specific Ionic Liquid and Their Photocatalytic Activities. Mat Lett.2011; 65: 3371–3373.Copyright (2011), with permeation from Elsevier)].

2. Influence of ionic liquids on the growth of nanofillers for electromagnetic-absorbing coatings

2.1. The fabrication of $BaCO_3$ nanostructures as nanofillers for electromagnetic-absorbing coatings

An economical and efficient ionic liquid-assisted chemical method was demonstrated for the first time for the fabrication of $BaCO_3$ nanostructures. The shape of these $BaCO_3$ nanostructures could be readily controlled by changing the chemical conditions and the amount of the chiral ionic liquid (CIL), ditetrabutylammonium tartrate, $[TBA]_2$[L-Tar] by Kowsari and coworkers [62]. The CIL is a reagent and templating agent for the fabrication of $BaCO_3$ nanostructures. It was demonstrated that $[TBA]_2$[L-Tar] served as a modifier in the reactionsystem.Figure 6 shows typical SEM images of $BaCO_3$ nanostructures synthesized with 0.05 g CIL at 170 °C for 24 h. From the SEM image Figure 6, it is clear that the typical $BaCO_3$ dendritic nanostructures assembled were hyacinth-like with rod-like nanostructures with lengths of up to several micrometers.

http://dx.doi.org/10.5772/51653

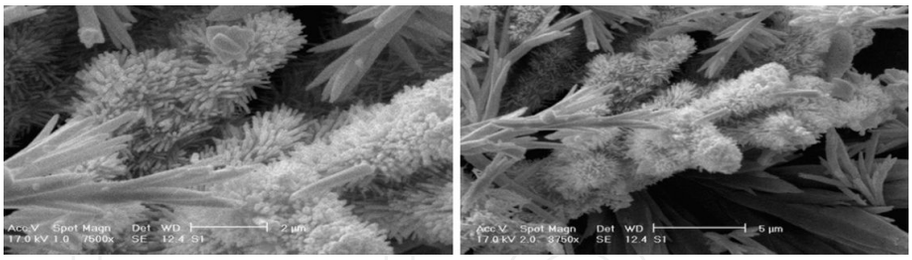

Figure 6. Typical scanning electron micrographs of $BaCO_3$ nanostructures synthesized with 0.05 g CIL, NaOH = 0.04 M (2 ml) at 170 °C for 24 h, the $Ba(NO_3)_2$ = 0.53 g. [Reproduced from Kowsari E, Karimzadeh AH. Using a Chiral Ionic Liquid for Morphological Evolution of $BaCO_3$ and its Radar Absorbing Properties as a Dendritic Nanofiller. Mat Lett. 2012;74, 33-36, Copyright (2012), with permeation from Elsevier)].

With increase in the amount of CIL to 0.1 g, flower-like $BaCO_3$ structures composed of dendritic petals were produced, which appeared as a result of oriented attachment and self-assembly, as exhibited in Fig 7.

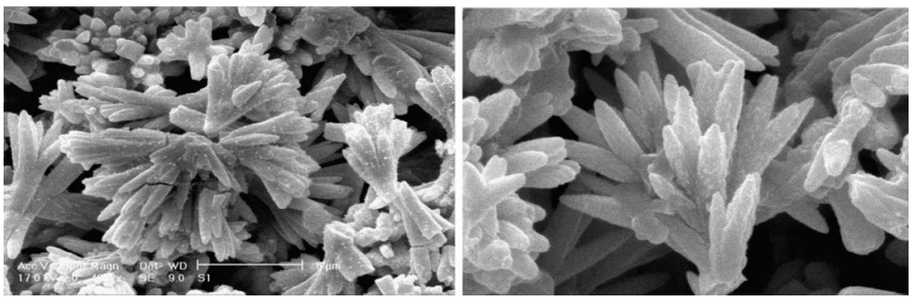

Figure 7. Typical scanning electron micrographs of $BaCO_3$ nanostructures synthesized with 0.1g CIL, NaOH = 0.04 M (2 ml) at 170 °C for 24 h, the $Ba(NO_3)_2$ = 0.53 g. [Reproduced from Kowsari E, Karimzadeh AH. Using a Chiral Ionic Liquid for Morphological Evolution of $BaCO_3$ and its Radar Absorbing Properties as a Dendritic Nanofiller. Mat Lett.2012;74, 33-36, Copyright (2012), with permeation from Elsevier)].

The effects of the synthetic parameters, such as the concentration of NaOH, reaction temperature, reaction time and $[Ba^{2+}]$, on the morphologies of the resulting products were investigated. Typical SEM images of the products with different morphologies brought about by varying the amount of NaOH are presented in Figure. 8.

Too much NaOH was found to be harmful to the formation of flower-like structures and resulted in atrophic flowers, which are analogs of a sphere as shown in Figure. 8. NaOH affected the reaction kinetics through tuning the dissolution-deposition equation of $Ba(OH)_2$, because soluble $Ba(NO_3)_2$ will first react with NaOH to form $Ba(OH)_2$ precipitate (Ksp) 1.09 × 10-15). The trend for $Ba(OH)_2$ to release Ba2+ decreased if the concentration of OH- is relatively high, leading to the thermodynamic change of nucleation and growth velocities, which is beneficial for the formation of spherical structures.

Figure 9 shows XRD patterns of the products obtained under different reaction conditions. It is clear that all of the peaks can be readily indexed to the pure orthorhombic phase of BaCO3 (JCPDS card no. 05-0378). The sharp diffraction peaks of the sample indicate that well-crystallized BaCO3 crystals can be easily obtained under the current syn-

thetic conditions. On comparing the XRD patterns of the four products, It was shown that the relative intensity of the peaks varied slightly.

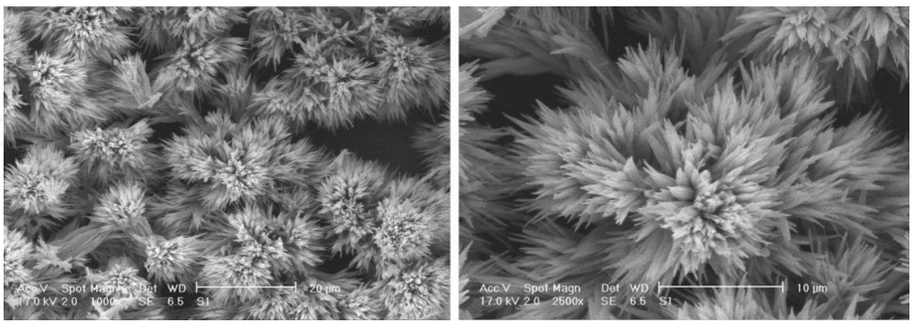

Figure 8. Typical scanning electron micrographs of $BaCO_3$ nanostructures synthesized with (a) 2.5 ml, CIL = 0.05 g at 170 °C for 24 h, $Ba(NO_3)_2$ = 0.53 g.] [Reproduced from Kowsari E, Karimzadeh AH. Using a Chiral Ionic Liquid for Morphological Evolution of $BaCO_3$ and its Radar Absorbing Properties as a Dendritic Nanofiller. Mat Lett.2012;74, 33-36, Copyright (2012), with permeation from Elsevier)].

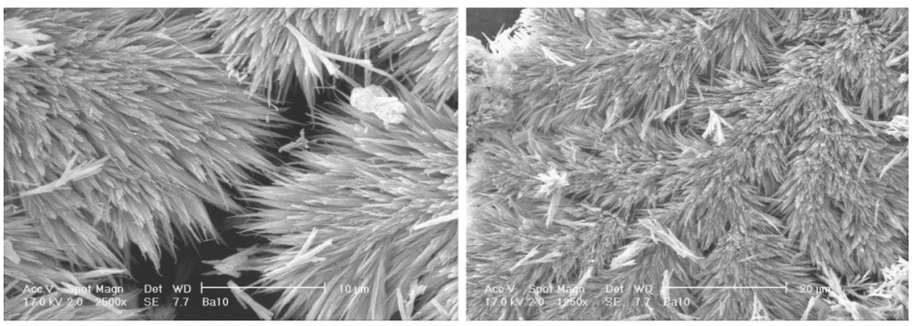

Figure 9. Typical scanning electron micrographs of $BaCO_3$ nanostructures synthesized with CIL = 0.05 g at 170 °C for 24 h, $Ba(NO_3)_2$ = 0.53 g. [Reproduced from Kowsari E, Karimzadeh AH. Using a Chiral Ionic Liquid for Morphological Evolution of $BaCO_3$ and its Radar Absorbing Properties as a Dendritic Nanofiller. Mat Lett.2012;74, 33-36, Copyright (2012), with permeation from Elsevier)].

The value of the minimum reflection loss for the $BaCO_3$ dendritic nanostructures composite was -40 dB at 10.2 GHz (for a thickness of 4.0 mm) [Figure. 10]. According to the results shown above, $BaCO_3$ dendritic nanostructures showed very strong absorption of microwave compared with other samples. It is noteworthy that the $BaCO_3$ dendritic nanostructures have special geometrical morphology. Such isotropic crystal symmetry can form isotropic quasi antennas and some continuous networks in the composites. It is possible for the electromagnetic waves to penetrate the nanocomposites formed by the numerous antenna-like semiconducting $BaCO_3$ dendritic nanostructures and for the energy to be induced into a dissipative current; then the current will be consumed in the continuous networks, which leads to the energy attenuation (19-20). More importantly, the interfacial electric polarization should be considered. However, further experimental and theoretical work is needed to clarify this mechanism.

http://dx.doi.org/10.5772/51653

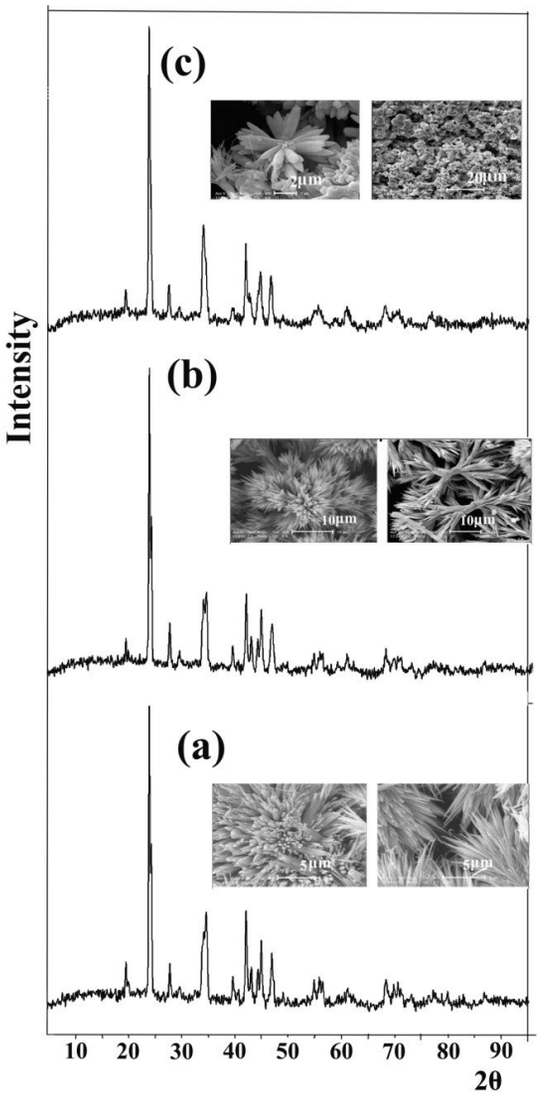

Figure 10. X-ray diffraction patterns of the $BaCO_3$ nanostructures synthesized with (a) 5 ml, (b) 2.5 ml, (NaOH (0.04 M) [CIL = 1.25 g /L at 170 °C for 24 h, $Ba(NO_3)_2$ = 13.25 g/L.], (c) 2.5 g/L CIL. [NaOH = 0.04 M (2 ml) at 170 °C for 24 h, the $Ba(NO_3)_2$ = 13.25 g/L]; [Reproduced from Kowsari E, Karimzadeh AH. Using a Chiral Ionic Liquid for Morphological Evolution of $BaCO_3$ and its Radar Absorbing Properties as a Dendritic Nanofiller. Mat Lett.2012;74, 33-36, Copyright (2012), with permeation from Elsevier)].

2.2. Fern-like, fish skeleton-like, bunched cubic, and butterfly-like BaO nanostructures as nanofillers for Radar-absorbing coatings

Fern-like, fish skeleton-like, bunched cubic, and butterfly-like BaO nanostructures have been synthesized by a hydrothermal method at 170 °C from $Ba(NO_3)_2$ •3H2O and NaOH in the presence of ammonium persulfate $(NH_4)_2S_2O_8$ (APS) by Kowsari and coworkers[63]. The effect of the chiral ionic liquid (CIL) ditetrabutylammonium tartrate, $[TBA]_2$[L-Tar], on the morphologies of the products has been investigated. It was demonstrated that $[TBA]_2$[L-Tar] served as a modifier in the reaction system. Furthermore, the BaO nanostructures have been used as fillers in high-performance microwave-absorbing coatings.

By controlling the concentrations of CIL, Ba^{2+}, and APS, shape transformations of the BaO could be achieved. When the amount of CIL was zero, rotor-like BaO was formed (Figure 11).

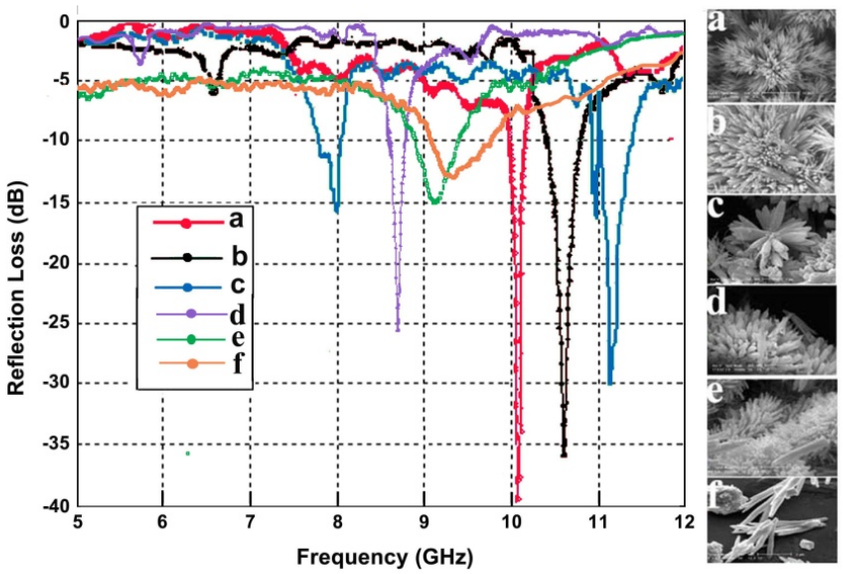

Figure 11. Reflection loss (dB) as a function of frequency (GHz) of $BaCO_3$ nanostructures synthesized with: (a) NaOH = 2.5 mL (0.04 M), CIL = 1.25 g /L for 24 h $Ba(NO_3)_2$ = 13.25 g/L; (b) NaOH = 5 mL (0.04 M) and CIL = 1.25 g /L for 24 h, $Ba(NO_3)_2$ = 13.25 g/L; (c) NaOH = 2 mL (0.04 M) and CIL = 2.5 g/L, for 24 h, amount of $Ba(NO_3)_2$ = 13.25 g/L; (d) NaOH = 2 mL (0.04 M), CIL = 1.25 g /L for 24 h, $Ba(NO_3)_2$ = 6.52 g/L; (e) NaOH = 2 mL (0.04 M), CIL = 1.25 g /L for 24 h, $Ba(NO_3)_2$ = 13.25 g/L; (f) NaOH- = 2 mL (0.04 M), CIL = 1.25 g /L for 48 h, $Ba(NO_3)_2$ = 13.25 g/L, (at 170 °C and with filler = 0.025 g in coating). [Reproduced from Kowsari E, Karimzadeh AH. Using a Chiral Ionic Liquid for Morphological Evolution of $BaCO_3$ and its Radar Absorbing Properties as a Dendritic Nanofiller. Mat Lett.2012;74, 33-36, Copyright (2012), with permeation from Elsevier)].

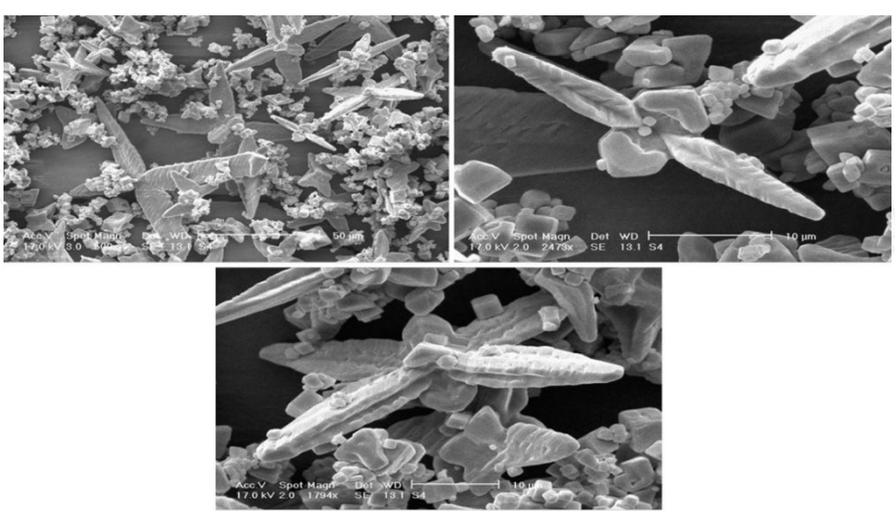

Figure 12. SEM images of products obtained with : 0.1 g CIL, keeping the reaction time fixed at 24 h; $Ba(NO_3)_2$ = 0.2 g, APS = 0.27 g, reaction temperature 170 °C. [Reproduced from Kowsari E, Karimzadeh AH. Fabrication of Fern-Like, Fish Skeleton-Like, and Butterfly-Like BaO Nanostructures as Nanofillers for Radar-Absorbing Nanocomposites. Mat Lett. 2012; 74:33–36, Copyright (2012), with permeation from Elsevier].

http://dx.doi.org/10.5772/51653

When the amount of CIL was increased gradually, while maintaining the same reaction time, rotor-like BaO changed to bunched cubic BaO, as shown in Figure 14. The cubes have a porous surface structure.

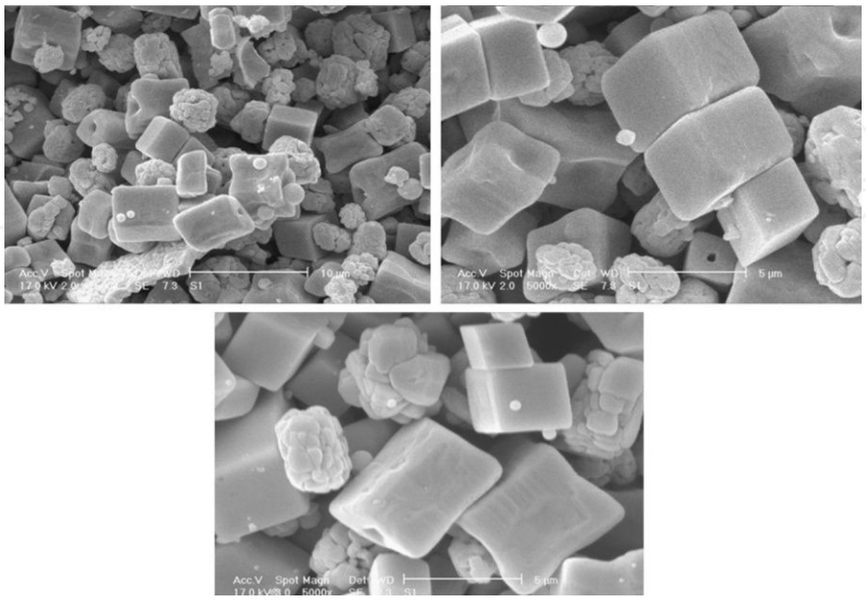

Figure 13. SEM images of products obtained with 0.1 g, CL= 0.15 g keeping the reaction time fixed at 24 h; $Ba(NO_3)_2$ = 0.2 g, APS = 0.27 g, reaction temperature 170 °C. [Reproduced from Kowsari E, Karimzadeh AH. Fabrication of Fern-Like, Fish Skeleton-Like, and Butterfly-Like BaO Nanostructures as Nanofillers for Radar-Absorbing Nanocomposites. Mat Lett.2012; 74:33–36, Copyright (2012), with permeation from Elsevier].

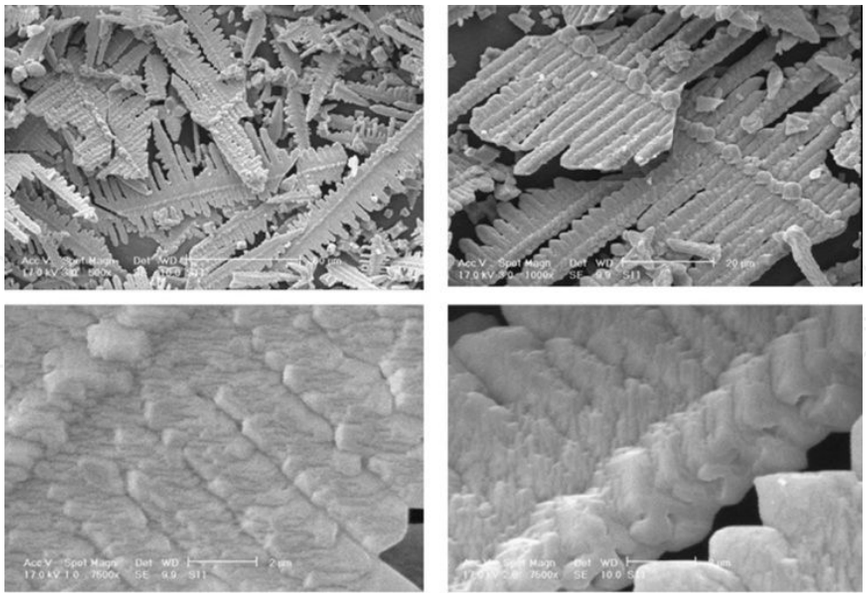

Figure 14. SEM images of products obtained with $Ba(NO_3)_2$ = 0.8 g, CIL = 0; APS = 0.27 g; (the reaction time was kept constant at 24 h and the reaction temperature was 170 °C). [Reproduced from Kowsari E, Karimzadeh AH. Fabrication of Fern-Like, Fish Skeleton-Like, and Butterfly-Like BaO Nanostructures as Nanofillers for Radar-Absorbing Nanocomposites. Mat Lett.2012; 74:33–36, Copyright (2012), with permeation from Elsevier].

The CIL clearly plays a key role in tailoring the form of the resultant BaO nanostructures. It is thought that hydrogen bonds formed between the hydrogen atom at the position-2 (connected to oxygen) of the CIL cation and the oxygen atoms of O–Ba crystal cores may act as effective bridges in connecting the produced BaO nuclei and CIL cations, playing a crucial role in the directional growth of the 2D nanocrystals.

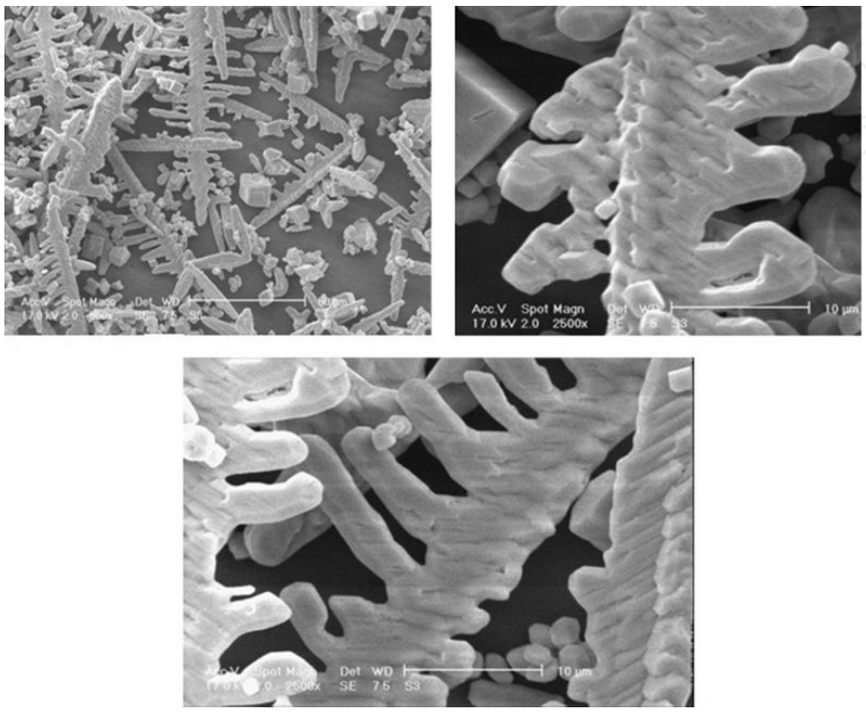

Figure 15. SEM images of products obtained with: $Ba(NO_3)_2$ = 0.4 g, CIL = 0, APS = 0.27 g; (the reaction time was kept constant at 24 h and the reaction temperature was 170 C). [Reproduced from Kowsari E, Karimzadeh AH. Fabrication of Fern-Like, Fish Skeleton-Like, and Butterfly-Like BaO Nanostructures as Nanofillers for Radar-Absorbing Nanocomposites. Mat Lett.2012; 74:33–36, Copyright (2012), with permeation from Elsevier].

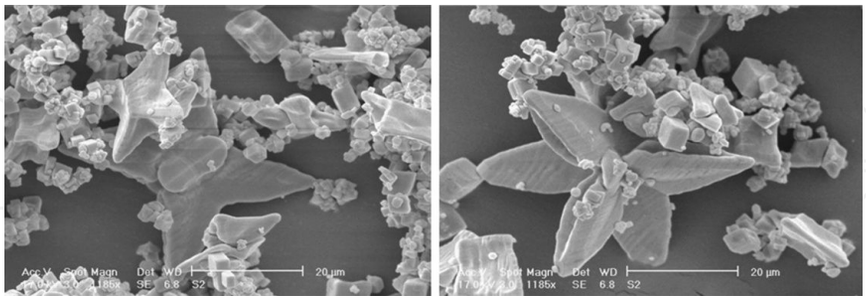

Figure 16. SEM images of products obtained with $Ba(NO_3)_2$ = 0.2 g, CIL = 0, APS = 0.27 g; (the reaction time was kept constant at 24 h and the reaction temperature was 170 C). [Reproduced from Kowsari E, Karimzadeh AH. Fabrication of Fern-Like, Fish Skeleton-Like, and Butterfly-Like BaO Nanostructures as Nanofillers for Radar-Absorbing Nanocomposites. Mat Lett.2012; 74:33–36, Copyright (2012), with permeation from Elsevier].

We also investigated the effect of the amount of $Ba(NO_3)_2$ on the morphology of the products. The respective products obtained from this series of experiments are depicted in Figure 13, 14, 15.

http://dx.doi.org/10.5772/51653

The value of the maximum reflection loss for the composite with BaO cubic nanostructures was measured as ⊚20 dB at 10.5 GHz for a thickness of 4.0 mm. According to the results shown in Figure 4, the BaO cubic nanostructures showed very strong absorption of microwaves compared with the other samples. It may be noted that the BaO cubic nanostructures had a special geometrical morphology.

2.3. Morphology evolution of the ZnO/Zn(OH)2 nanofillers using ionic liquids

An efficient ionic-liquid-assisted chemical method for the fabrication of $ZnO/Zn(OH)_2$ nanoplates is demonstrated by kowsari and coworkers [64]. The shape of the resulting $ZnO/Zn(OH)_2$ nanostructures could be readily controlled by changing the chemical conditions and the amount of $[Cn(mim)]^+$ $H2PO_{4-}$ as a task-specific ionic liquid (TSIL). The TSIL thus serves as a reagent and templating agent for the fabrication of $ZnO/Zn(OH)_2$ nanoplates. Furthermore, a possible growth mechanism of the $ZnO/Zn(OH)_2$ nanostructures is proposed. The effects of different morphologies of the nanofillers on electromagnetic properties have been investigated.

By controlling the concentration of the TSIL and the reaction time, shape transformations of the $ZnO/Zn(OH)_2$ nanostructures could be achieved. Our results show that the quantity of the TSIL affected the morphology of the $Zn(OH)_2$ and caused changes in the interplanar separation and the arrangement of the nanoplates. Salient SEM images are compared in Fig. 1. In this figure, it can be seen that as the quantity of the TSIL was increased from 0.1 g to 0.2 g, the separation between the nanoplates decreased and the number of nanoplates increased.

The TSIL clearly played a key role in tailoring the form of the resultant $ZnO/Zn(OH)_2$ nanocomposites.To analyze the effect of the reaction time on morphology, the reaction was carried out for 12, 24, and 48 h, while keeping the amounts of Zn2+ and TSIL constant. Fig. 2 shows the morphologies of the products. It can be seen that with increasing reaction time, the separation between the nanoplates increased and the number of nanoplates decreased

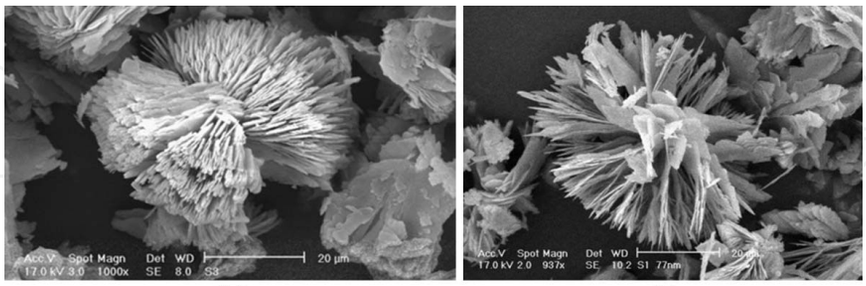

(a) (b)

Figure 17. SEM images of products obtained with different time of reaction: (a) 12 h, (b) 48 h, $Zn(NO_3)_2$ = 0.8 g, OH = 0.27 g, reaction temperature 170 °C, TSIL =0.1 g.

Fig. 18 clearly shows the process of TSIL-assisted hydrothermal growth of ZnO and Zn(OH)2 crystals. The amount of the growth unit $[Zn(OH)_2(H_2PO_4)2]^{2-}$ is greatly increased, and further ZnO and $Zn(OH)_2$ nuclei directly conglomerate to form a two-dimensional

nanosheet structure in order to lower the surface potential. Thereafter, the nanosheets self-assemble to produce a cabbage-like structure.

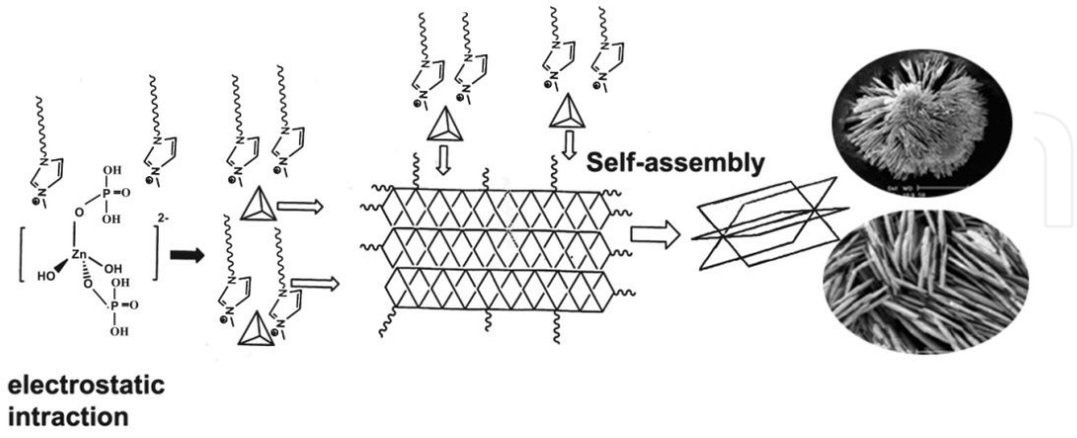

Figure 18. Schematic illustration of the processes of $Zn(OH)_2$/ZnO nanostructure assembly by IL-assisted hydrothermal growth.

The TSIL clearly played a key role in tailoring the form of the resultant ZnO/$Zn(OH)_2$ nanocomposites. In a general manner, the produced coatings showed broadband absorber behavior, which may be attributed to the dielectric properties and the particular shape of the $Zn(OH)_2$/ZnO nanofillers. When radar impinges on a radar -absorbing coating, the incident radiation is not totally absorbed immediately. The radar attenuation by the radar-absorbing coating is significantly complex and different attenuation mechanisms can occur. Equal amounts of three types of $Zn(OH)_2$/ZnO nanostructures with different morphologies and different separations between their nanoplates, as synthesized under different conditions, were used as fillers in coatings.

The value of the maximum reflection loss for the composite with $Zn(OH)_2$/ZnO nanostructures was measured ~20 dB at 8 GHz for a thickness of 4.0 mm. The samples incorporating $Zn(OH)_2$/ZnO nanostructures of a morphology with a shorter inter-plate separation displayed higher absorptions. The absorption was also shifted toward higher frequencies. Moreover, a higher bandwidth was observed. It may be noted that the ZnO/$Zn(OH)_2$ nanostructures had a special geometrical morphology, namely that of a multi-layer microwave absorber. More importantly, the interfacial electric polarization should be considered. It is well known that the permittivity mainly originates from electronic polarization, ion polarization, and intrinsic electric-dipole polarization, on which the crystal structure, size, and shape of nanomaterials may have important influences. On the basis of the electron microscopy characterization results, we can conclude that the radar-absorbing properties are associated with the crystal structure, the crystallization, and the degree of aggregation of the nanocrystal building blocks. This also explains why the ZnO/$Zn(OH)_2$ nanostructures studied here show different radar-absorption properties. However, further experimental and theoretical work is needed to clarify the mechanism.

http://dx.doi.org/10.5772/51653

3. Conclusion

Over the past years, there has been an increasing interest in developing hierarchically structural materials on a nanometer scale due to their novel or enhanced properties. By controlling the condition of reaction, shape transformations of the resulting hierarchical ceramic nanomaterials could be achieved. In this chapter, the ceramic nanomaterials have been synthesized in a single reaction system by simply adjusting the reaction conditions and used as fillers in high-performance microwave-absorbing coatings, with epoxy resin as the polymer matrix. The task specific ionic liquids thus serves as a reagent or templating agent for the fabrication of ceramic oxides. The effects of different morphologies of the nanofillers on electromagnetic properties have been investigated. The maximum reflection attenuation was measured as −20 dB in the frequency range 5−12 GHz.

Author details

Elaheh Kowsari*

Address all correspondence to: kowsarie@aut.ac.ir

Department of Chemistry, Amirkabir University of Technology, Tehran, Iran

References

[1] Balanis, C. A. (1989). *Advanced Engineering Electromagnetics*, New York, John Wiley and Sons.

[2] Lee, S. M. (1991). *International Encyclopedia of Composites*, New York, VCH Publishers.

[3] Clark, D. E., Diane, C. F., Stephen, J. O., & Richards, S. (1995). *Microwaves: Theory and Application in Materials Processing III*, Westerville, The American Ceramic Society.

[4] Hippel, A. (1954). *Dielectric Materials and Applications*, London, Artech House.

[5] Yusoffa, A. N., Abdullah, M. H., Ahmad, S. H., Jusoh, S. F., Mansor, A. A., & Hamid, S. A. A. (2002). Electromagnetic and absorption properties of some microwave absorbers. *J.Appl Phy*, 92(2), 876-882.

[6] Orfanidis, S. J. (2008). *Electromagnetic Waves and Antennas*, Available from, http://www.ece.rutgers.edu/~orfanidi/ewa/, accessed Oct.

[7] Sucher, M. ., & Fox, J. (1963). *Handbook of the microwave measurements* (3 ed.), New York, John Wiley and Sons.

[8] Thostenson, E. T., & Chou, T. W. (1999). Microwave processing: fundamentals and applications. *Composites: Part A: Applied Science and Manufacturing*, 30(9), 1055-1071.

[9] Jarem, L. M., Johnson, J. B. ., & Scott, W. (1995). Measuring the permittivity and permeability of sample at Ka Band using a partially flled waveguide. *IEEE Transactions on Microwave and Techniques*, 43(12), 2654-2667.

[10] Watts, P. C. P., Hsu, P. C. P., Barnes, W. K., & Chambers, A. (2003). B High Permittivity from Defective Multiwalled Carbon Nanotubes in the X-Band. *Adv Mater.*, 15(7-8), 600-603.

[11] Wadhawan, A., Garrett, D., & Perez, J. M. (2003). Nanoparticle-assisted microwave absorption by single-wall carbon nanotubes. *Appl Phys Lett.*, 83(13), 2683-2685.

[12] Deng, L. J., & Han, M. (2007). Microwave Absorbing Performances of Multiwalled Carbon Nanotube Composites with Negative Permeability. *Appl Phys Lett.*, 91(2), 023119-023121.

[13] Liu, J. R., Itoh, M., Terada, M., Horikawa, T., & Machida, K. I. (2007). Enhanced Electromagnetic Wave Absorption Properties of Fe Nanowires in Gigaherz Range. *Appl Phys Lett*, 91(9), 093101-093103.

[14] Chen, Y. J., Cao, M. S., Wang, T. H., & Wan, Q. (2004). Microwave absorption properties of the ZnO nanowire-polyester composites. *Appl. Phys. Lett.*, 84(17), 3367-3370.

[15] Tang, Z., & Kotov, N. A. (2005). One-dimensional assemblies of nanoparticles: Preparation, properties, and promise. *AdV Mater.*, 17(8), 951-962.

[16] Murphy, C., Sau, T. K., Gole, A. M., Orendorff, C. J., Gao, J., Gou, L., Hunyadi, S., & Li, T. (2005). Anisotropic Metal Nanoparticles: Synthesis, Assembly, and Optical Applications. *J. Phys. Chem. B*, 109(29), 13857-13870.

[17] Xia, Y., & Halas, N. (2005). Shape-Controlled Synthesis and Surface Plasmonic Properties of Metallic Nanostructures. *J MRS Bull.*, 30(5), 338-348.

[18] Liz-Marza´n, L. M. (2006). Tailoring Surface Plasmons through the Morphology and Assembly of Metal Nanoparticles. *Langmuir*, 22(1), 32-41.

[19] Link, S., & El -Sayed, M. A. (1999). Spectral Properties and Relaxation Dynamics of Surface Plasmon Electronic Oscillations in Gold and Silver Nanodots and Nanorods. *J. Phys. Chem. B*, 103(40), 8410-8426.

[20] Vasilev, K., Zhu, T., Wilms, M., Gillies, G., Lieberwirth, I., Mittler, S., Knoll, W., & Kreiter, M. I. (2005). One-step Synthesis of Gold Nanowires in Aqueous Solution. *Langmuir*, 21(26), 12399-12403.

[21] Wiley, B., Sun, Y., Mayers, B., & Xia, Y. (2005). Shape-Controlled Synthesis of Metal Nanostructures: The Case of Silver. *Chem Eur J*, 11(2), 454-463.

[22] Giersig, M., Pastoriza-Santos, I., & Liz-Marza´n, L. M. (2004). Evidence of an Aggregative Mechanism During the Formation of Silver Nanowires in N,N-dimethylformamide. *J Mater Chem*, 14, 607-610.

[23] Umar, A. A., & Oyama, M. (2006). Formation of Gold Nanoplates on Indium Tin Oxide Surface: Two-Dimensional Crystal Growth from Gold Nanoseed Particles in the Presence of Poly(vinylpyrrolidone). *Cryst Growth Des.*, 6(4), 818-821.

[24] Shankar, S. S., Rai, A., Ankamwar, B., Singh, A., Ahmad, A., & Sastry, M. (2004). Biological Synthesis of Triangular Gold Nanoprisms. *Nat Mater*, 3(7), 482-488.

[25] Xiong, Y., Mc Lellan, J. M., Chen, J., Yin, Y., Li, Z., & Xia, Y. (2005). Kinetically Controlled Synthesis of Triangular and Hexagonal Nanoplates of Palladium and Their SPR/SERS Properties. *J Am Chem Soc.*, 127(48), 17118-17127.

[26] Yang, J., Lu, L., Wang, H., Shi, W., & Zhang, H. (2006). Glycyl Glycine Templating Synthesis of Single-Crystal Silver Nanoplates. *Cryst Growth Des.*, 6(9), 2155-2158.

[27] Sun, Y., & Xia, Y. (2002). Shape-Controlled Synthesis of Gold and Silver Nanoparticles. *Science*, 298(5601), 2176-2179.

[28] Yu, D., & Yam, V. W. (2004). Controlled Synthesis of Monodisperse Silver Nanocubes in Water. *J. Am Chem Soc.*, 126(41), 13200-13201.

[29] Gou, L., & Murphy, C. J. (2005). Fine-Tuning the Shape of Gold Nanorods. *Chem. Mater.*, 17(14), 3668-3672.

[30] Chen, S., Wang, Z. L., Ballato, J., Foulger, S. H., & Carrol, D. L. (2003). Monopod, Bipod, Tripod, and Tetrapod Gold Nanocrystals. *J Am ChemSoc.*, 125(52), 16186-16187.

[31] Sau, T. K., & Murphy, C. J. (2004). Room Temperature, High-Yield Synthesis of Multiple Shapes of Gold Nanoparticles in Aqueous Solution. *J Am Chem Soc*, 126(28), 8648-8649.

[32] Yamamoto, M., Kashiwagi, Y., Sakata, T., Mori, H., & Nakamoto, M. (2005). Synthesis and Morphology of Star-Shaped Gold Nanoplates Protected by Poly(N-vinyl-2-pyrrolidone). *Chem Mater.*, 17(22), 5391.

[33] Kuo, C., & Huang, M. H. (2005). Synthesis of Branched Gold Nanocrystals by a Seeding Growth Approach. *Langmuir*, 21(5), 2012-2016.

[34] Hao, E., Bailey, R. C., Schatz, G. C., Hupp, J. T., & Li, S. (2004). Synthesis and Optical Properties of "Branched" Gold Nanocrystals. *Nano Lett.*, 4(2), 327-330.

[35] Bakr, O. M., Wunsch, B. H., & Stellacci, F. (2006). High-Yield Synthesis of Multi-Branched Urchin-Like Gold Nanoparticles. *Chem Mater.*, 18(14), 3297-3301.

[36] Burt, J. L., Elechiguerra, J. L., Reyes-Gasga, J., Montejano-Carrizales, J. M., & Yacaman, M. J. (2005). Beyond Archimedean Solids: Star Polyhedral Gold Nanocrystals. *J Cryst Growth*, 285(4), 681-691.

[37] Wang, T., Hu, X., & Dong, S. (2006). Surfactantless Synthesis of Multiple Shapes of Gold Nanostructures and Their Shape-Dependent SERS Spectroscopy. *J Phys Chem. B*, 110(34), 16930-16936.

[38] Ma, H., Huang, S., Feng, X., Zhang, X., Tian, F., Yong, F., Pan, W., Wang, Y., & Chen, S. (2006). Electrochemical Synthesis and Fabrication of Gold Nanostructures Based on Poly(N-vinylpyrrolidone). *Chem Phys Chem;*, 7(2), 333-335.

[39] Shen, G. Z., Bando, Y., & Golberg, D. (2007). Self-Assembled Hierarchical Single-Crystalline β-SiC Nanoarchitectures. *Cryst Growth Des.*, 7(1), 35-38.

[40] Teng, X. W., & Yang, H. (2005). Synthesis of platinum multipods: an induced anisotropic growth. *Nano Lett.*, 5(5), 885-891.

[41] Liu, B., & Zeng, H. C. (2004). Fabrication of ZnO "Dandelions" via a Modified Kirkendall Process. *J Am Chem Soc.*, 126(51), 16744-16746.

[42] Xie, S. H., & Zhao, D. Y. (2002). A Simple Route for the Synthesis of Multi-Armed CdS Nanorod-Based Materials. *Adv Mater.*, 14(21), 1537-1540.

[43] Zhang, Z., Sun, H., Shao, X., Li, D., Yu, H., & Han, M. (2005). Three-Dimensionally Oriented Aggregation of a Few Hundred Nanoparticles into Monocrystalline Architectures. *Adv Mater.*, 17(1), 42-47.

[44] Kowsari, E., & Faraghi, G. (2010). Synthesis by an ionic liquid assisted method and optical properties of nanoflower Y_2O_3. *J Mater Res Bull*, 45, 939-945.

[45] Murray, C. B., Kagan, C. R., & Bawendi, M. G. (1995). Self-Organization of CdSe Nanocrystallites into Three-Dimensional Quantum Dot Superlattices. *Science*, 270(5240), 1335-1338.

[46] Andreas, T. (2004). CuCl Nanoplatelets from an Ionic Liquid-Crystal Precursor. *Angew Chem Int. Ed. Engl.*, 43(40), 5380-5382.

[47] Jiang, Y., & Zhu, Y. J. (2005). Microwave-Assisted Synthesis of Sulfide M2S3 (M = Bi, Sb) Nanorods Using an Ionic Liquid. *J Phys Chem., B*, 109(10), 4361-4364.

[48] Jiang, J., Yu, S. H., Yao, W. T., Ge, H., & Zhang, G. Z. (2005). Morphogenesis and Crystallization of Bi_2S_3 Nanostructures by an Ionic Liquid-Assisted Templating Route: Synthesis, Formation Mechanism, and Properties. *Chem. Mater.*, 17(24), 6094-6100.

[49] Jiang, Y., Zhu, Y. J., & Cheng, G. F. (2006). Synthesis of Bi_2Se_3 Nanosheets by Microwave Heating Using an Ionic Liquid Cryst Growth Des. 9, 2174-2176.

[50] Nskashima, T., & Kimizuka, N. (2003). Interfacial Synthesis of Hollow TiO_2 Microspheres in Ionic Liquids. *J Am Chem Soc.*, 125(21), 6386-6387.

[51] Rai, P., Jo, J. N., Lee, I. H., & Yu, Y. T. (2010). Fabrication of 3D rotorlike ZnO nanostructure from 1D ZnO nanorods and their morphology dependent photoluminescence property. *J Solid State Sci*, 12, 1703-1710.

[52] Patzke, G. R., Krumeich, F., & Nesper, R. (2002). Oxidic Nanotubes and Nanorods-Anisotropic Modules for a Future Nanotechnology Angew. *Chem., Int. Ed. Engl.*, 41(14), 2446-2461.

http://dx.doi.org/10.5772/51653

[53] Cui, Y., & Lieber, C. M. (2001). Functional Nanoscale Electronic Devices Assembled Using Silicon Nanowire Building Blocks. *Science*, 291(5505), 851-853.

[54] Chen, A. C., Peng, X. P., Koczkur, K., & Miller, B. (2004). Super-hydrophobic tin oxide nanoflowers. *Chem Commun.*, 1964-1965.

[55] Gur, I., Fromer, N. A., Geier, M. L., & Alivisatos, A. P. (2005). Air-stable all-inorganic nanocrystal solar cells processed from solution. *Science*, 310(5747), 462-465.

[56] Antonietti, M., Kuang, D. B., Smarsly, B., & Yong, Z. (2004). Ionic liquids for the convenient synthesis of functional nanoparticles and other inorganic nanostructures. *Angew ChemInt Ed*, 43(38), 4988-4992.

[57] Xu, X., Zhang, M., Feng, J., & Zhang, M. (2008). Shape-controlled Synthesis of Single-Crystalline Cupric Oxide by Microwave Heating Using an Ionic Liquid. *Mat Lett.*, 62(17-18), 2728-2790.

[58] Ma, L., Chen, W. X., Li, H., Zheng, Y. F., & Xu, Z. D. (2008). Ionic Liquid-Assisted Hydrothermal Synthesis of MoS_2 Microspheres. *Mat Lett.*, 62(6-7), 797-799.

[59] Liu, X., Peng, P., Ma, J., & Zheng, W. (2009). Preparation of Novel CdSe Microstructure by Modified Hydrothermal Method. *Mat Lett.*, 63(8), 673-675.

[60] Kowsari, E., & Ghezelbash, M. R. (2012). Ionic Liquid-Assisted, Facile Synthesis of ZnO/SnO_2 Nanocomposites, and Investigation of Their Photocatalytic Activity. *Mat Lett.*, 68, 17-20.

[61] Kowsari, E., & Ghezelbash, Mohammad Reza. (2011). Synthesis of cactus-like zincoxysulfide (ZnO_xS_{1-x}) nanostructures assisted by a task-specific ionic liquid and their photocatalytic activities. *Mat Lett.*, 65-3371.

[62] Kowsari, E., & Karimzadeh, A. H. (2012). Using a Chiral Ionic Liquid for Morphological Evolution of $BaCO_3$ and its Radar Absorbing Properties as a Dendritic Nanofiller. *Mat Lett.*, 74, 33-36.

[63] Kowsari, E., & Karimzadeh, A. H. (2012). Fabrication of Fern-Like, Fish Skeleton-Like, and Butterfly-Like BaO Nanostructures as Nanofillers for Radar-Absorbing Nanocomposites. *Mat Lett.*, 74, 33-36.

IntechOpen